LITHOS 482-483 (2024) 107698

Contents lists available at ScienceDirect

LITHOS

journal homepage: www.elsevier.com/locate/lithos

# How old is the Eye of Africa? A polyphase history for the igneous Richat Structure, Mauritania

El Houssein Abdeina [a,*], Fred Jourdan [b], Gilles Chazot [c,*], Hervé Bertrand [d], Bernard Le Gall [c]

[a] Department of Geology, Faculty of Sciences and Techniques, University of Nouakchott Al-Aasriya, BP 5026, Nouakchott, Mauritania
[b] Western Australian Argon Isotope Facility, School of Earth and Planetary Sciences and John de Laeter Centre, Curtin University, Perth, Australia
[c] Laboratoire Geo-Ocean, Institut Universitaire Européen de la Mer, Université de Brest (UBO), UMR 6538, place Copernic, 29280, Plouzané, France
[d] Laboratoire de Géologie de Lyon, Ecole Normale Supérieure de Lyon, Université Lyon 1, CNRS UMR 5276, Université de Lyon, Lyon, France

ARTICLE INFO

*Keywords:*
Richat
Eye of Africa
Mauritania
Gabbros
$^{40}Ar/^{39}Ar$ age
Central Atlantic Magmatic Province

ABSTRACT

The annular Richat Structure, in Mauritania, is among the most striking geological features on Earth visible from space. Nicknamed "the Eye of Africa", its intriguing concentric shaping has drawn attention for several decades. Formerly hypothesized as an astrobleme, it is now consensually recognized as a complex igneous intrusion, involving two ring-like gabbroic bodies, a central breccia and carbonatite dykes. However, the coexistence of until now undated tholeiitic gabbros and 99 Ma carbonatites akin to alkaline magmatism remained enigmatic.

We provide the first plagioclase $^{40}Ar/^{39}Ar$ age determination and new geochemical data on the gabbroic bodies. Although no robust age was obtained, numerical modelling of our results suggests that the gabbros were intruded between 230 and 200 Ma. This age bracket is compatible with the ~200 Ma Central Atlantic Magmatic Province (CAMP). Moreover, the compositions of these tholeiitic gabbros match the two chemical groups of the CAMP the best represented in northwest Africa. Therefore, we argue that the Richat gabbros correspond to two CAMP sills intruded conformably into the Late Proterozoic/Lower Paleozoic sedimentary sequences of the Taoudenni basin. About 100 My later, the gabbros and their country rocks were locally uplifted by an alkaline intrusion (expressed now on surface by the carbonatites), resulting in a circular doming, 40 km in diameter. The subsequent erosion led to the actual flattened concentric structure. Therefore, the Richat Structure represents a two-stage igneous-history, separated by a time lapse of ~100 My, resulting in two CAMP gabbroic sills mimicking ring-like bodies.

## 1. Introduction

The circular Richat Structure is one of the most famous geological features on Earth so far photographed from space since the first orbital satellites were launched in the fifties. Located in the sedimentary basin of Taoudenni in Mauritania, it corresponds to an eroded dome, 40 km in diameter, involving many concentric ring-like structures, giving it its name "the Eye of Africa". Beyond its stunning visual aspect, its origin has long been discussed and is still a matter of debates. Although the hypothesis of a meteorite impact crater has long been ruled out in favour of a magmatic origin (Dietz et al., 1969), the chronology of the formation of this structure and the age of some igneous formations are still largely unknown. In this study, we provide new chronological and geochemical data about the gabbros, the most prominent igneous formation of the Richat Structure.

## 2. Geological and structural setting

The ring-like Richat Structure is made of several concentric crests of late Proterozoic/Lower Paleozoic hard sandstone and quartzitic sandstone layers intercalated with softer mudstones (Fig. 1). Two flat-bottomed depressions with significant salt deposits (sebkra) are present in the centre and south of the structure. The centre of the depression is occupied by a breccia 3 km in diameter and up to 40 m thick. It is composed of polymictic fragments (sandstones, stromatolithic limestones) embayed in a quartz/feldspar-rich matrix. The breccia is highly silicified. Analcimolites, rocks made of >75% of analcime, are present in the SW and NE parts of the central depression and form crests up to 3.5 m thick above the sebkra surface. They are principally made of analcime, calcite, iron oxides and zeolites, in addition to angular quartz grains. Gabbroic rocks are also present as two of the most central ring

* Corresponding authors.
*E-mail address:* Gilles.Chazot@univ-brest.fr (G. Chazot).

https://doi.org/10.1016/j.lithos.2024.107698
Received 24 February 2024; Received in revised form 12 June 2024; Accepted 12 June 2024
Available online 15 June 2024

structures. The ca. 70 m-wide outer ring (Tin Jouker) is located 7–8 km from the centre, while the 30 m-wide inner one (Guelb Richat) is only 3 km from the centre. The Richat intrusive complex also comprises a swarm of >60 carbonatite dykes, from 0.30 to 1.5 m-thick and mostly orientated in the range N10–30°E, that cut at high angle the regional ring structure (Woolley et al., 1984). Most of them occurred in the southern half of the structure. They are systematically highly weathered and contain many xenoliths of sedimentary country-rocks (Sedigh et al., 2024). Two carbonatite necks were also recognized in the central part of the depression (Poupeau et al., 1996). Kimberlitic rocks described from a trench made by Ashton Mining in the northern part of the Richat Structure (Matton and Jébrak, 2014) are no longer exposed at the surface. Their presence at shallow depth has been recently confirmed by magnetic records (Abdeina et al., 2021). The circular Richat Structure is cut by a network of variously-oriented faults, striking predominantly at N10°E, N90°E and N160°E, and displaying for most of them an extensional component (Fig. 1).

Due to its spectacular appearance, especially from space, the origin

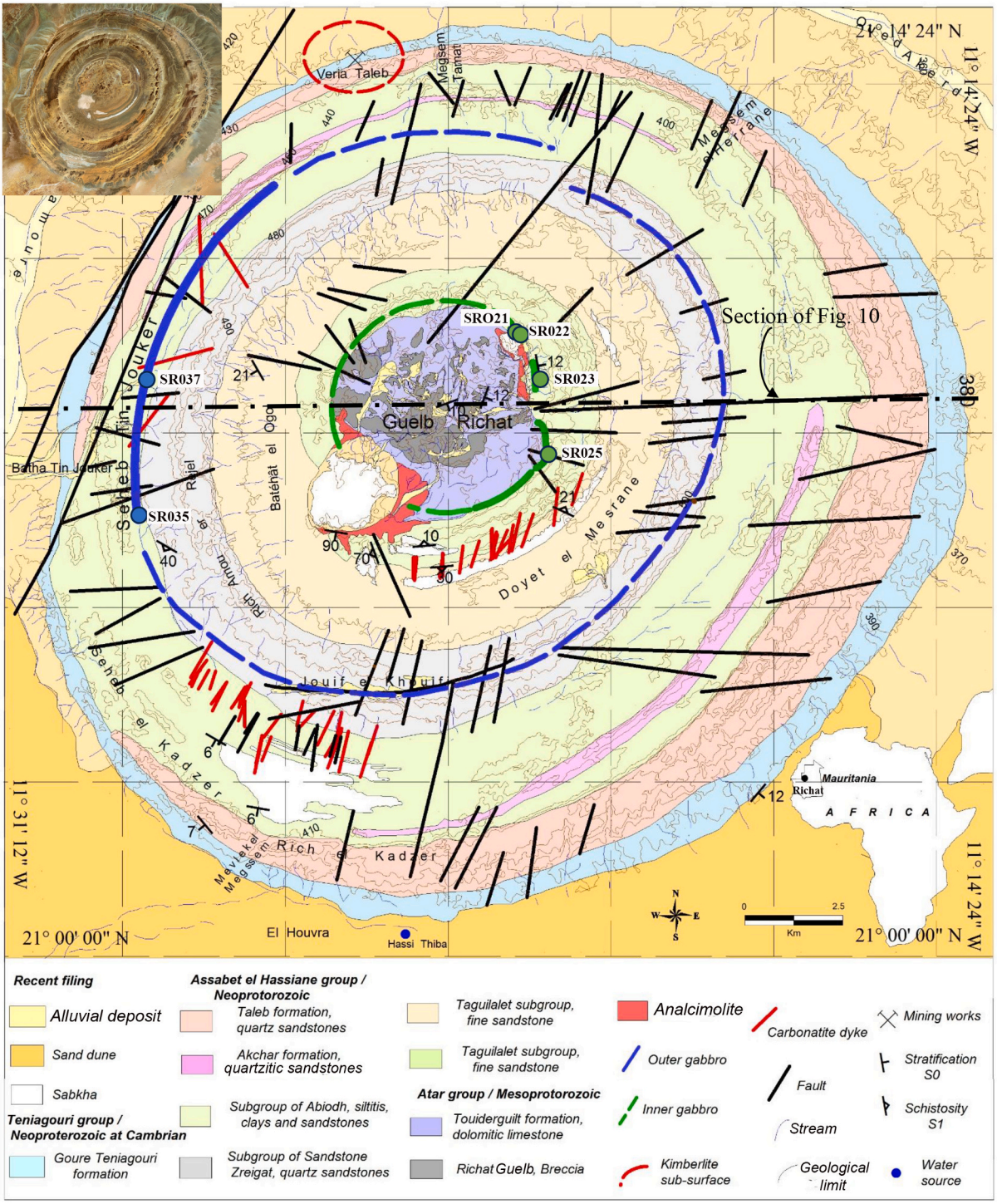


**Fig. 1.** Geological map of the Richat structure. The sample numbers refer to the gabbros analysed in this study. Insert: sketch map of Africa showing the location of the Richat structure in Mauritania (modified from O'Connor et al., 2004). The trace of the cross-section in Fig. 10 is drawn. The upper left inset shows a satellite image of the Richat Structure (Image from Google Earth).

of the Richat Structure has long been investigated and disputed. The meteorite impact model formerly proposed by Cailleux et al. (1964) was later discarded and substituted by igneous models which imply a shallow central intrusion that caused the up-doming of the sedimentary country-rocks and a network of sill/dyke bodies that possibly fed a volcanic activity at the surface (Abdeina et al., 2021; Dietz et al., 1969; Matton et al., 2005; Matton and Jébrak, 2014; O'Connor et al., 2004; Trompette, 1968).

Hovever, there are still unresolved issues about the nature, relationships and origin of some Richat igneous and sedimentary components whose recognition is hindered by the pervasive hydrothermal alteration processes experienced by the whole area. Two disputable issues concern the two gabbroic intrusions. They have been considered by some authors as sills, based on their apparently concordant relationships with the sedimentary country rocks (O'Connor et al., 2004; Trompette, 1968), whereas others favour ring-dyke structures, based on their circular geometry (Abdeina et al., 2021; Matton and Jébrak, 2014). However, the sand cover precludes unambiguous contact observations. The atypical spatial association of gabbros of tholeiitic affinity (Matton and Jébrak, 2014; Trompette, 1968) with carbonatites (Woolley et al., 1984), and kimberlites (Matton and Jébrak, 2014) usually related to alkaline magmas remains also unsolved. Matton and Jébrak (2014) tentatively explained this unusual association by the coeval rise of tholeiitic magmas from the subcontinental lithospheric mantle and alkaline magmas from the asthenosphere. However, radioisotopic dating of the gabbroic rocks was missing to definitely check the validity of this hypothesis.

Futhermore, the central breccia has been attributed to a karst collapse post-dating a hydrothermally induced dissolution of limestone layers (Matton et al., 2005). Yet, the relationships between this breccia and the igneous events is still unclear.

More controversial are the nature and origin of the central analcimolites. While it is consensually accepted that they seem to be the product of a strong hydrothermal alteration, whether they derive from rhyolites (Bidaut and Durandau, 1962; Bardossy et al., 1963; Fudali, 1973; Matton and Jébrak, 2014) or from lacustrine sediments (Trompette, 1968; Boussaroque, 1975; O'Connor et al., 2004) is still a matter of debates.

## 3. Previous geochronology with inference on emplacement history

The first absolute chronological data obtained on the Richat igneous rocks by Poupeau et al. (1996) from fission tracks analyses of apatites in carbonatitic rocks (one neck and two dykes) gave an integrated age of 99 ± 5 Ma for their emplacement. Note that these authors discarded a fission track age of apatite at 85 ± 5 Ma previously obtained by the same team on a carbonatite dyke (Netto et al., 1992), because of suspected irradiation problems.

Moreover, an unpublished age of ca. 99 Ma was obtained by Asthon Mining Inc. on the northern kimberlitic plug (quoted in Matton and Jébrak, 2014). This age is coeval to the carbonatite age, but information on the dating method is not available so it remains to be validated.

Matton et al. (2005) obtained an age of 98.2 ± 2.6 Ma using $^{40}Ar/^{39}Ar$ on K-feldspars extracted from grey sediments associated with the central breccia. This age was consistent with the fission track ages yielded by the carbonatites (Poupeau et al., 1996). Consequently, they interpreted the whole Richat Structure as resulting from a doming process induced at depth by a ca. 100 Ma-old alkaline complex, coeval with an important hydrothermal process which in turn produced karstification and breccias in the centre of the structure.

Notwithstanding the limited geochronological data, Matton and Jébrak (2014) proposed an emplacement model for the Richat complex implying a large tholeiitic magma chamber that fed (undated) gabbroic ring dykes shortly before the arrival of deep alkaline magmas forming the carbonatitic dykes and the kimberlite plug. At a third stage, felsic silicate melts derived from the underlying magma chamber would form the presumed central rhyolites (i.e. now analcimolites). According to these authors, all these events were thought to occur in <10 My at around 100 Ma.

The aim of this paper is to provide the first $^{40}Ar/^{39}Ar$ data on the gabbroic ring-like bodies and to investigate their geochemistry in order to better constrain the Richat igneous history and to solve the enigma of supposedly coexisting tholeiitic and carbonatitic magmas.

## 4. Analytical methods

*Major and trace elements*: Whole-rock major elements on gabbros were measured on the Horiba-Jobin–Yvon-Ultima 2 ICP-AES at the IUEM (European Institute for Marine Studies, Pôle de Spectrométrie Océan, Brest, France). The detailed description of the analytical procedure is given in Cotten et al. (1995). Major elements were determined from an $H_3BO_3$ solution, boron being used as internal standard for ICP-AES analysis. For major elements, relative standard deviation is 1% for $SiO_2$ and 2% for the other major elements.

Trace element concentrations were measured with a Thermo Element2 HR-ICP-MS in Brest (France), after a repeated HF-$HClO_4$ digestion, and $HNO_3$ dilution (see Li and Lee, 2006 for details). The repeated analysis of the international standard BCR2 demonstrated an external reproducibility better than 5–10% depending on the element and concentration. All the data are presented in Table 1.

*$^{40}Ar/^{39}Ar$ geochronology*: Plagioclase crystals were separated from the 150–215 μm fraction using a Frantz isodynamic magnetic separator and were hand-picked grain-by-grain under the binocular stereomicroscope. Plagioclase crystals were further leached using diluted HF (2 N) for 5 min and thoroughly rinsed in distilled water and loaded in two separated discs, along with unrelated samples. The plagioclase sample was irradiated for 40 h alongside Fish Canyon standards (Jourdan and Renne, 2007), for which an age of 28.294 Ma (± 0.13%) was used (Renne et al., 2011). The discs were Cd-shielded (to minimize undesirable nuclear interference reactions) and irradiated in the Oregon State university nuclear reactor (USA) in central position. The mean J-values computed from standard grains within the small pits are given in Supplementary Material (Sup. Mat. 1, 2). Mass discrimination was monitored regularly through the analysis using an automated air pipette and relative to an air ratio of 298.56 ± 0.31 (Lee et al., 2006) and values are provided in Supplementary Material. The correction factors for interfering isotopes were $(^{39}Ar/^{37}Ar)$ Ca = 6.95 × 10 $^{-4}$ (± 1.3%), $(^{36}Ar/^{37}Ar)$ Ca = 2.65 × 10 $^{-4}$ (± 0.84%) and $(^{40}Ar/^{39}Ar)$ K = 7.30 × 10 $^{-4}$ (± 12.4%; Renne et al., 2013). The $^{40}Ar/^{39}Ar$ analyses were performed at the Western Australian Argon Isotope Facility at Curtin University. Plagioclase crystal populations were step-heated using a continuous 100 W PhotonMachine© $CO_2$ (IR, 10.6 μm) laser fired on the crystals during 60 s. Each of the standard crystals was fused in a single step.

The gas was purified in an extra low-volume stainless steel extraction line of 240 cc and using one SAES AP10 and one GP50 getter. Ar isotopes were measured in static mode using a low volume (600 cc) ARGUS VI mass spectrometer from Thermofisher© set with a permanent resolution of ~200. Measurements were carried out in multi-collection mode using four faradays to measure mass 40 to 37 and an ultra-low-background compact discrete dynode ion counter to measure mass 36. We measured the relative abundance of each mass simultaneously using 10 cycles of peak-hopping and 33 s of integration time for each mass. Detectors were calibrated to each other electronically and using Air shot beam signals. The raw data were processed using the ArArCALC software (Koppers, 2002) and the ages have been calculated using the decay constants recommended by Renne et al. (2011). Blanks were monitored every 3 to 4 steps. All parameters and relative abundance values are provided in Supplementary Material and have been corrected for blank, mass discrimination and radioactive decay. Individual errors in Supplementary Material are given at the 1σ level.

**Table 1**
Major and trace elements for gabbros.

| | SR-021 | SR-022 | SR-023 | SR-025 | SR-034 | SR-035 | SR-037 |
|---|---|---|---|---|---|---|---|
| | | Inner ring | | | | Outer ring | |
| Major elements (wt%) | | | | | | | |
| $SiO_2$ | 51.49 | 51.51 | 50.61 | 51.45 | 50.13 | 50.57 | 51.41 |
| $TiO_2$ | 0.93 | 0.94 | 0.81 | 0.96 | 0.90 | 0.98 | 1.02 |
| $Al_2O_3$ | 14.99 | 15.32 | 16.29 | 15.28 | 14.64 | 15.92 | 16.10 |
| $Fe_2O_{3T}$ | 10.13 | 10.14 | 9.99 | 10.43 | 10.55 | 10.38 | 10.33 |
| MnO | 0.16 | 0.16 | 0.15 | 0.17 | 0.21 | 0.19 | 0.17 |
| MgO | 7.68 | 7.24 | 4.84 | 7.26 | 7.58 | 6.55 | 6.42 |
| CaO | 10.81 | 10.69 | 10.36 | 10.56 | 8.97 | 11.02 | 10.98 |
| $Na_2O$ | 2.12 | 2.18 | 2.68 | 2.20 | 2.99 | 2.28 | 2.33 |
| $K_2O$ | 0.73 | 0.81 | 1.87 | 0.81 | 1.22 | 0.65 | 0.56 |
| $P_2O_5$ | 0.14 | 0.15 | 0.21 | 0.15 | 0.09 | 0.10 | 0.13 |
| LOI | 0.76 | 0.89 | 2.38 | 0.58 | 2.40 | 1.51 | 0.85 |
| Total | 99.93 | 100.04 | 100.19 | 99.85 | 99.70 | 100.15 | 100.32 |
| Trace elements (ppm) | | | | | | | |
| Be | 0.79 | | | 0.82 | | 0.70 | 0.72 |
| V | 258 | | | 266 | | 271 | 268 |
| Cr | 513 | | | 364 | | 80.0 | 80.0 |
| Mn | 1361 | | | 1387 | | 1566 | 1445 |
| Co | 47.3 | | | 46.5 | | 44.3 | 43.6 |
| Ni | 101 | | | 91 | | 83 | 80 |
| Cu | 91 | | | 99 | | 113 | 109 |
| Zn | 73 | | | 78 | | 133 | 103 |
| Ga | 18.53 | | | 19.09 | | 20.57 | 20.40 |
| Rb | 23.92 | | | 27.12 | | 19.49 | 17.92 |
| Sr | 228 | | | 229 | | 197 | 210 |
| Y | 19.43 | | | 20.64 | | 19.56 | 20.72 |
| Zr | 88.5 | | | 89.8 | | 78.2 | 88.2 |
| Nb | 10.1 | | | 10.3 | | 4.9 | 6.1 |
| Mo | 0.79 | | | 0.85 | | 1.12 | 0.96 |
| Ba | 541 | | | 362 | | 188 | 195 |
| La | 12.43 | | | 13.47 | | 9.17 | 9.97 |
| Ce | 25.78 | | | 28.38 | | 20.26 | 22.17 |
| Pr | 3.31 | | | 3.60 | | 2.76 | 3.03 |
| Nd | 13.94 | | | 15.14 | | 12.34 | 13.60 |
| Sm | 3.16 | | | 3.40 | | 3.05 | 3.31 |
| Eu | 1.11 | | | 1.16 | | 1.13 | 1.16 |
| Gd | 3.52 | | | 3.83 | | 3.46 | 3.77 |
| Tb | 0.59 | | | 0.62 | | 0.59 | 0.64 |
| Dy | 3.50 | | | 3.73 | | 3.52 | 3.79 |
| Ho | 0.72 | | | 0.77 | | 0.72 | 0.77 |
| Er | 1.99 | | | 2.12 | | 1.97 | 2.11 |
| Tm | 0.30 | | | 0.32 | | 0.30 | 0.32 |
| Yb | 1.99 | | | 2.10 | | 1.91 | 2.05 |
| Lu | 0.29 | | | 0.31 | | 0.28 | 0.29 |
| Hf | 2.74 | | | 2.90 | | 2.53 | 2.72 |
| Ta | 0.89 | | | 0.95 | | 0.48 | 0.49 |
| W | 0.31 | | | 0.34 | | 0.32 | 0.29 |
| Pb | 3.36 | | | 3.54 | | 22.24 | 19.81 |
| Th | 2.45 | | | 2.54 | | 1.92 | 1.86 |
| U | 0.54 | | | 0.57 | | 0.33 | 0.38 |

Our criteria for the determination of plateau are as follows: plateaus must include at least 70% of $^{39}Ar$. The plateau should be distributed over a minimum of 3 consecutive steps agreeing at 95% confidence level and satisfying a probability of fit (P) of at least 0.05.

## 5. Petrographic and geochemical data

Three samples from the outer gabbro and four samples from the inner gabbro were collected (Fig. 1). They display rather similar doleritic (subophitic) textures (Fig. 2). Their paragenesis is dominated by ca. 50% of plagioclase (labradorite - bytownite, in the range $An_{61–70}$ $Ab_{27–37}$ $Or_{0.7–1.2}$, associated with ca. 25% of clinopyroxene (both augite-diopside and pigeonite ($En_{36-54}$ $W_{21–47}Fs_{10–36}$, $En_{44-57}$ $W_{9-13}Fs_{35–44}$, respectively) and ca. 10% of orthopyroxene ($En_{54-79}$ $W_{4-5}Fs_{17–41}$). 5–7% of large anhedral Fe—Ti oxides are present. Graphic intergrowths of quartz and feldspar (micropegmatite) occur in small interstitial pockets. Minor amounts of secondary amphibole and biotite are observed, but no zircon has been observed in these samples. These mineral characteristics, in particular the presence of pigeonite and the chemical composition of the augitic clinopyroxenes according to the Ti vs Ca + Na diagram of Leterrier et al. (1982), are typical of continental tholeiites.

Major element compositions are very homogeneous (Table 1), with $SiO_2$ ranging from 50.1 to 51.5 wt%. The gabbros are moderately differentiated (MgO from 7.68 to 4.84 wt%). Their $TiO_2$ and $P_2O_5$ contents, ranging from 0.81 to 1.02 wt% and from 0.09 to 0.21 wt%, respectively, classify them as low-Ti continental tholeiites (Fig. 3). They are enriched in light rare earth elements (LREE) relative to middle REE (MREE) and heavy REE (HREE) (Fig. 4a). They are also enriched in large ion lithophile elements (LILE), with a positive Pb anomaly (Fig. 4b). These characteristics are similar to those described by Matton and Jébrak (2014). More in detail, the outer and inner gabbros share the same MREE to HREE patterns, but the inner gabbros display a stronger LREE and LILE enrichment, with a marked Ba positive anomaly, whereas the outer gabbros exhibit a stronger Pb positive anomaly and a distinct Nb—Ta negative anomaly.

## 6. Geochronological data

Two samples were selected for $^{40}Ar/^{39}Ar$ age determination, based on the lowest LOI value, namely SR037 (LOI = 0.85 wt%) from the outer gabbro and SR025 (LOI = 0.58 wt%) from the inner gabbro (Fig. 1). None of the two samples yielded an accurate age and the data are not easily interpretable either. The SR037 argon release spectrum shows a tilde-shape structure with the low-temperature extraction steps hovering around ~200 Ma while the higher temperature extraction steps smilingly converge toward ages of 225–230 Ma (Fig. 5a). The shape of the age spectra is roughly mirrored by the K/Ca plot with the youngest and older steps being associated with high and low K/Ca ratios, respectively. Such a tilde-shape is usually attributed to sericite alteration after plagioclase (Jiang et al., 2021; Verati and Jourdan, 2014). The inverse isochron plot fails to produce an isochron but the data trend does not suggest the presence of excess Ar. SR025 yielded a very unstructured age spectrum with step ages ranging from ca. 220 Ma to >500 Ma (Fig. 5b). The K/Ca plot shows a tilde-shape spectrum suggesting alteration by sericite. The inverse isochron reveals a dominant trend toward a $^{40}Ar/^{36}Ar$ trapped ratio > 3000 clearly indicating the presence of excess Ar.

## 7. Discussion

### 7.1. Age of the Richat gabbros

Although neither an accurate nor a precise isotopic age of the tholeiitic intrusions can be obtained, plagioclase $^{40}Ar/^{39}Ar$ data from sample SR037 still contains useful geochronological information. To interpret the data, we propose two scenarios involving alteration and excess $^{40}Ar^*$ along with a third scenario which involves both processes.

Scenario 1: providing no excess $^{40}Ar^*$ is present, the tilde-shape of the K/Ca ratio spectrum suggests that the sample has been slightly altered as can be seen in the thin section images of Fig. 2. According to sericite/plagioclase mixing experiment and alteration numerical modelling (Jiang et al., 2021; Verati and Jourdan, 2014), this indicates in turn that the youngest steps having their apparent ages decreased to ca. 200 Ma, are closer to the age of the alteration event, while the older steps converge toward an apparent age of >225 Ma, which in this case, would represent a minimum age for the intrusions. To test this hypothesis, we carried out numerical simulations to model a mixture of plagioclase affected by thermal diffusive loss and younger sericite with two distinct domain sizes, using the ArArDiff algorithm (Jourdan et al., 2017; Jourdan and Eroglu, 2017). We followed the approach and parameters used in Jiang et al. (2021) and modelled resulting age and K/

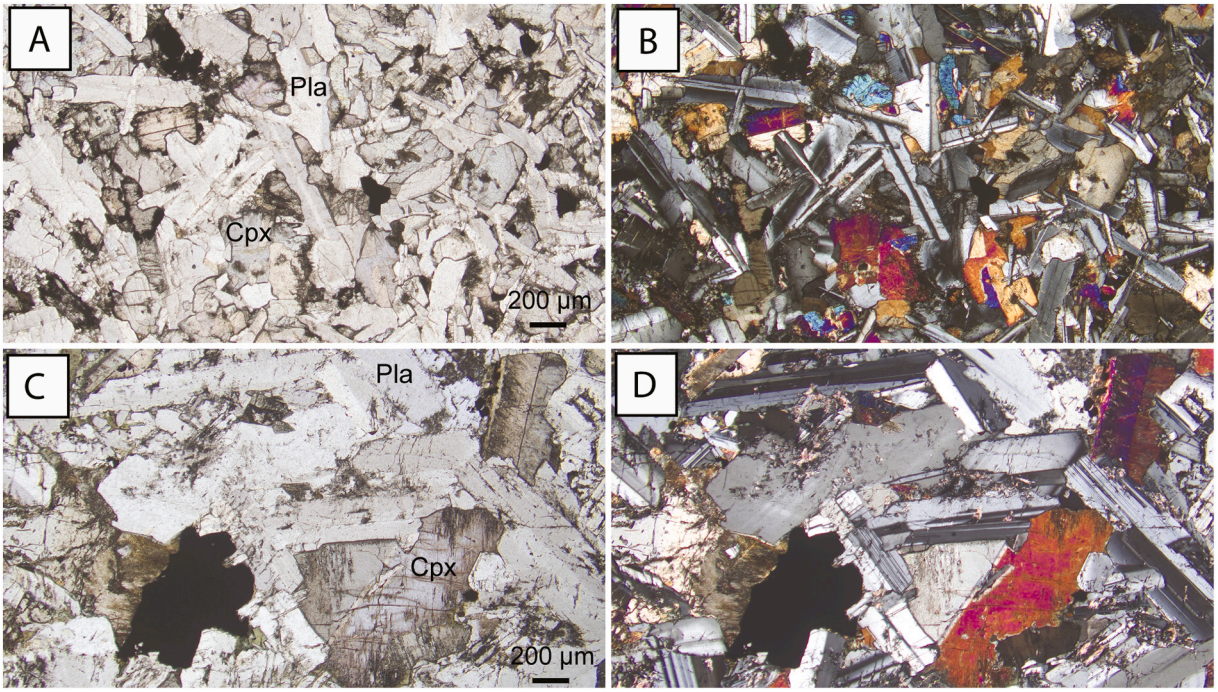


**Fig. 2.** Photomicrographs showing the inner (SR025, A and B) and outer (SR037, C and D) gabbros in plane-polarized light (A and C) and crossed-polarized light (B and D).

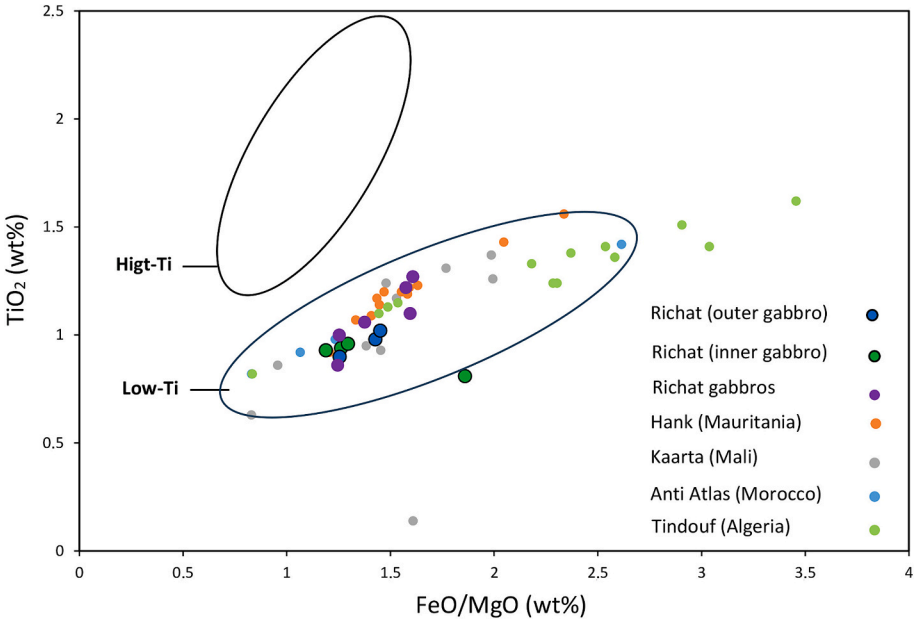


**Fig. 3.** $TiO_2$ versus FeO/MgO diagram showing the Richat outer and inner gabbros compared to the Central Atlantic Magmatic Province (CAMP) gabbros from Hank and Kaarta (Boscaini et al., 2022), Tindouf (Hachemaoui et al., 2022) and from Moroccan Anti-Atlas (Marzoli et al., 2019). Richat gabbros in purple are from Matton (2008). The low-Ti and high-Ti fields are from Albarede (1992). (For interpretation of the references to colour in this figure legend, the reader is referred to the web version of this article.)

Ca $^{40}Ar/^{39}Ar$ spectra here using an intrusion age of 230 Ma and a hydrothermal alteration age of 100 Ma, the latter corresponding to the age of the alkaline magmatism within the Richat Structure (Poupeau et al., 1996). All the characteristics of our model are given in in Table S1. Our model successfully reproduces the age spectrum derived from the data (Fig. 6a). Our model works to some extent, also for the K/Ca spectrum although we note that it is somewhat less successful in reproducing the exact shape of the K/Ca spectrum (Fig. S1). This suggests that our model is plausible but might be oversimplified to reproduce the complex size distributions of sericite affecting the K/Ca ratio in plagioclase.

Scenario 2: an alternative hypothesis is that any trace of alteration has been successfully eliminated during the hand-picking process, as this is often the case with relatively fresh plagioclase (Jiang et al., 2021), and that the oldest steps are associated with a small amount of excess $^{40}Ar^*$ degassed at high-temperature steps (Scibiorski et al., 2021). We use ArArDiff to illustrate this possibility and where only 0.01% of excess Ar

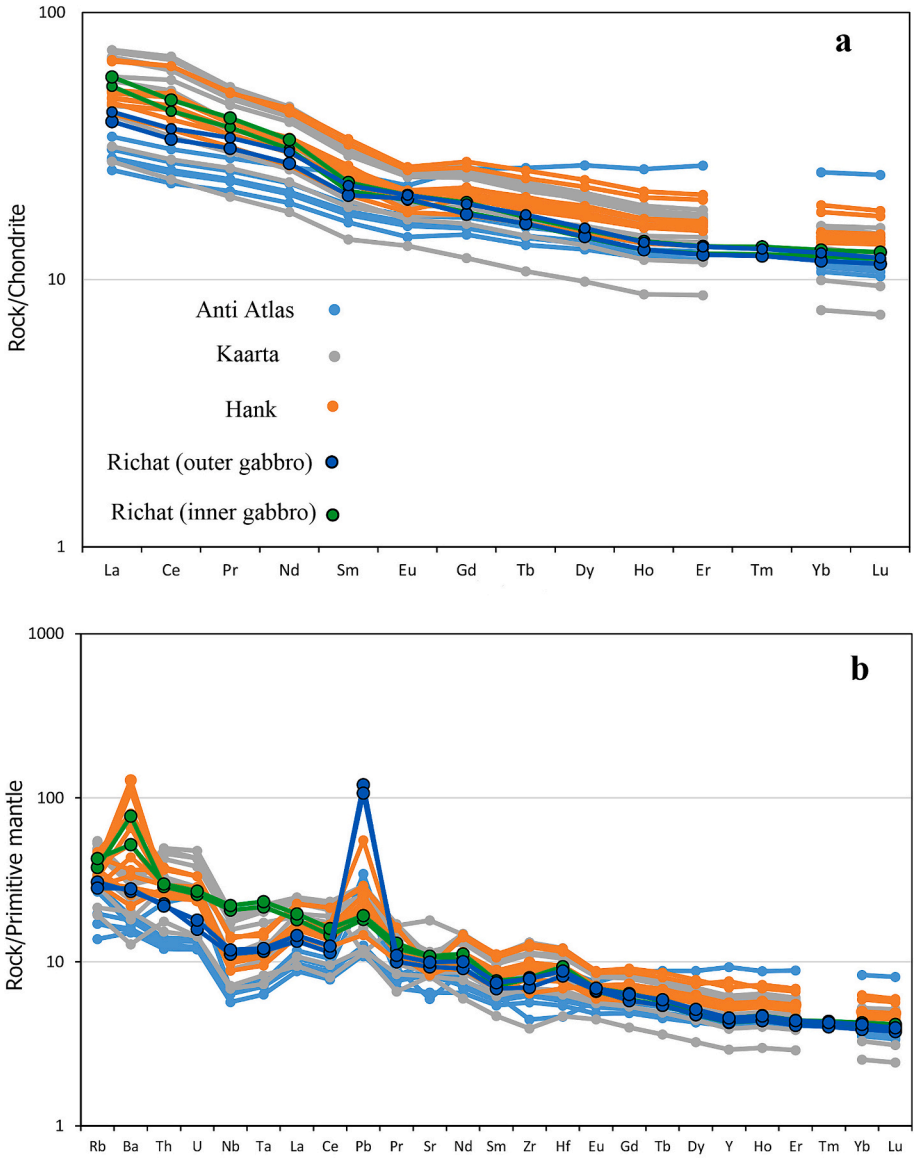


**Fig. 4.** Chondrite normalized REE (a) and primitive mantle normalized incompatible element patterns (b) of Richat gabbros compared to CAMP gabbros (same references as in Fig. 3). Patterns normalized after McDonough and Sun (1995).

(with an arbitrary "age" of 2 Ga) is hosted in minute clinopyroxene inclusions (cf. Table S1 for parameters). Once again, we successfully reproduce the shape of the age spectrum (Fig. 6b). This hypothesis would therefore suggest that the age of the intrusion is around ~200 Ma, such as the widely reported Central Atlantic Magmatic Province (CAMP; Fig. 7) (Boscaini et al., 2022; Davies et al., 2017; Verati et al., 2005). Such a scenario would explain the anomalous older steps with individual error ages of ~245 Ma and the presence of excess $^{40}$Ar* in this sample would be in agreement with the large amount of excess $^{40}$Ar* identified in the neighbouring sample SR025. The issue in this case is that excess Ar* in minute amount of clinopyroxene does not modify the K/Ca ratio to any visible extent and thus cannot account for the tilde-shape K/Ca plot (Fig. S1).

Scenario 3: a third possibility is a combination of both of these scenarios where excess Ar and alteration are mixed. In this case, the alteration phase is best approximated with an event slightly younger than the emplacement of the magma (i.e. magma-induced hydrothermal fluids affected the rocks immediately to up to a few million years after crystallization). Here we demonstrated the plausibility of this scenario by using crystallization ages of 201.5 Ma coupled with alteration ages of 200 and 100 Ma corresponding to *syn*-intrusion hydrothermal alteration (e.g. Jourdan et al., 2009) and hydrothermal alteration associated with the Richat alkaline magmatism, respectively. (Fig. 6c, d, respectively). We also used the same characteristics for excess $^{40}$Ar* as in scenario 2, and only one domain of sericite (cf. Table S1*)*. The numerical models associated with this scenario work well to reproduce the small error-plateau encountered with the low-temperature extraction steps but, like for scenario 1, are only approximately reproducing the K/Ca spectrum (Fig. S1) although the best model-data fit so far for the Ca/K plot is perhaps obtained for scenario 3b, with both a crystallization and alteration age of ~200 Ma.

The numbers used in all our numerical models are approximate and meant to be illustrative only. As such, we don't have any mean to differentiate between the three scenarios, although scenarios 1 and 3 seem the most likely due to the shape of the K/Ca plot. Finally, we note that SR025 age spectrum is too complex to be interpreted safely due to large amount of excess $^{40}$Ar*, but we note that the lowest temperature extraction steps are the least affected by excess Ar and similarly converge toward ca. 220 Ma. Whichever of three hypotheses is retained, numerical modelling and plagioclase $^{40}$Ar/$^{39}$Ar systematics suggest that

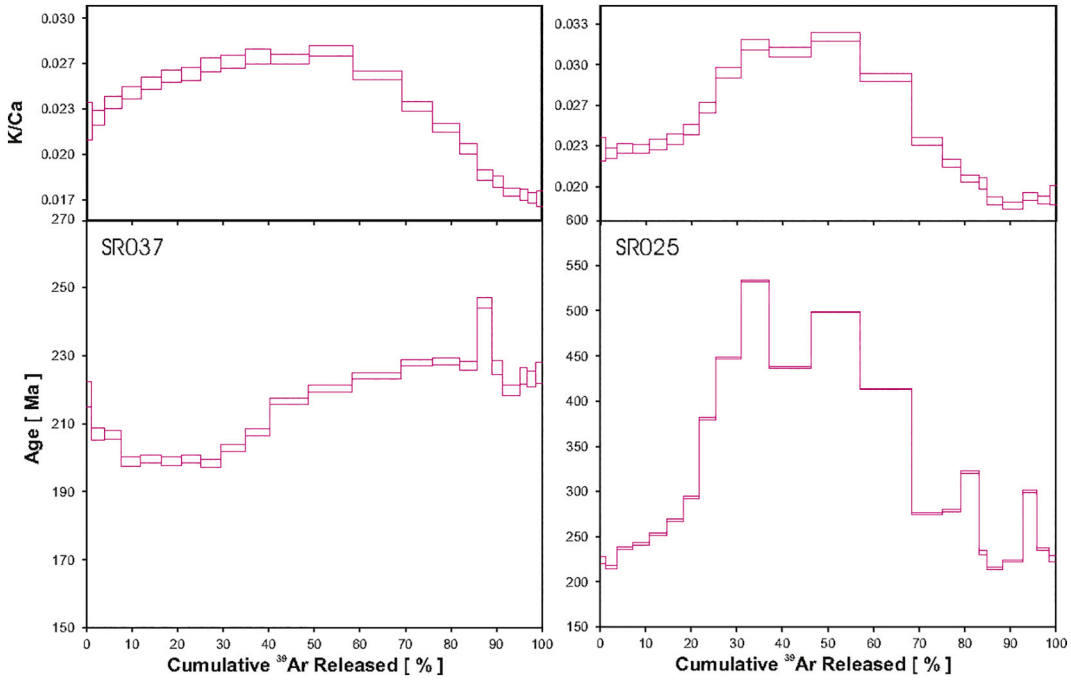


**Fig. 5.** Step-heating $^{40}Ar/^{39}Ar$ age and K/Ca spectra for sample SR037 and SR025.

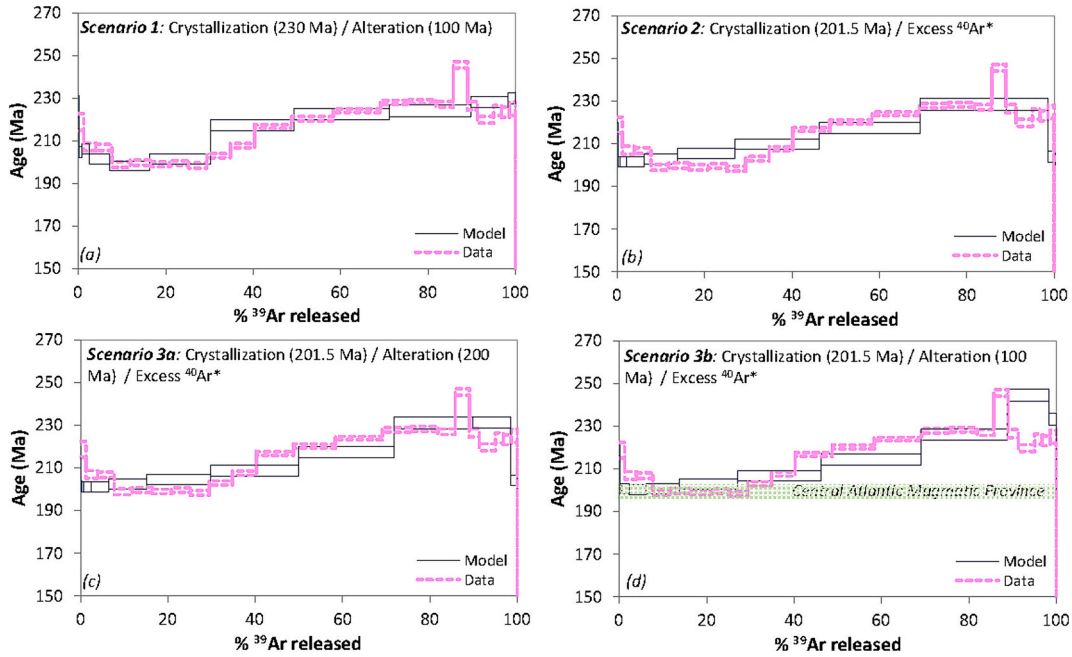


**Fig. 6.** ArArDIFF modelled $^{40}Ar/^{39}Ar$ age spectra (shown in solid-line blue boxes) of that simulate the age mixing between the primary plagioclase and younger sericite produced after the alteration of plagioclase (cf. Jiang et al., 2021) and/or the incorporation of excess $^{40}Ar^*$, or both. Actual data from sample SR037 (Fig. 5a) are shown in dashed-line pink boxes for comparison. Scenario 1: Crystallization = 230 Ma; Alteration = 100 Ma. Scenario 2: Crystallization = 201.5 Ma + Excess $^{40}Ar^*$. Scenario 3a: Crystallization = 201.5; Alteration = 200 Ma + Excess $^{40}Ar^*$. Scenario 3b: Crystallization = 201.5 Ma; Alteration = 100 Ma + Excess $^{40}Ar^*$. All parameters and thermal histories are given in Table S1. (For interpretation of the references to colour in this figure legend, the reader is referred to the web version of this article.)

the tholeiitic gabbro was intruded sometimes between ca. 230 and 200 Ma.

In summary, the igneous Richat Structure was previously considered as formed during a single event, lasting a few My around 100 Ma, based only on the few available ages obtained on the carbonatitic dykes (Poupeau et al., 1996), on the kimberlite plug (in Matton and Jébrak, 2014) and on the sediments in the central breccia (Matton et al., 2005). Our new results instead show that the Richat Structure formed during two distinct igneous episodes separated by a time-interval of ca. 100 My. This finding allows us to shed light on two outstanding issues dealing with: i) the significance of coexisting tholeiitic and carbonatitic/alkaline magmas and ii) the structural significance of the juxtaposed circular (ring-like) gabbroic intrusions and the network of N10–30°E carbonatitic dykes crosscutting the whole structure.

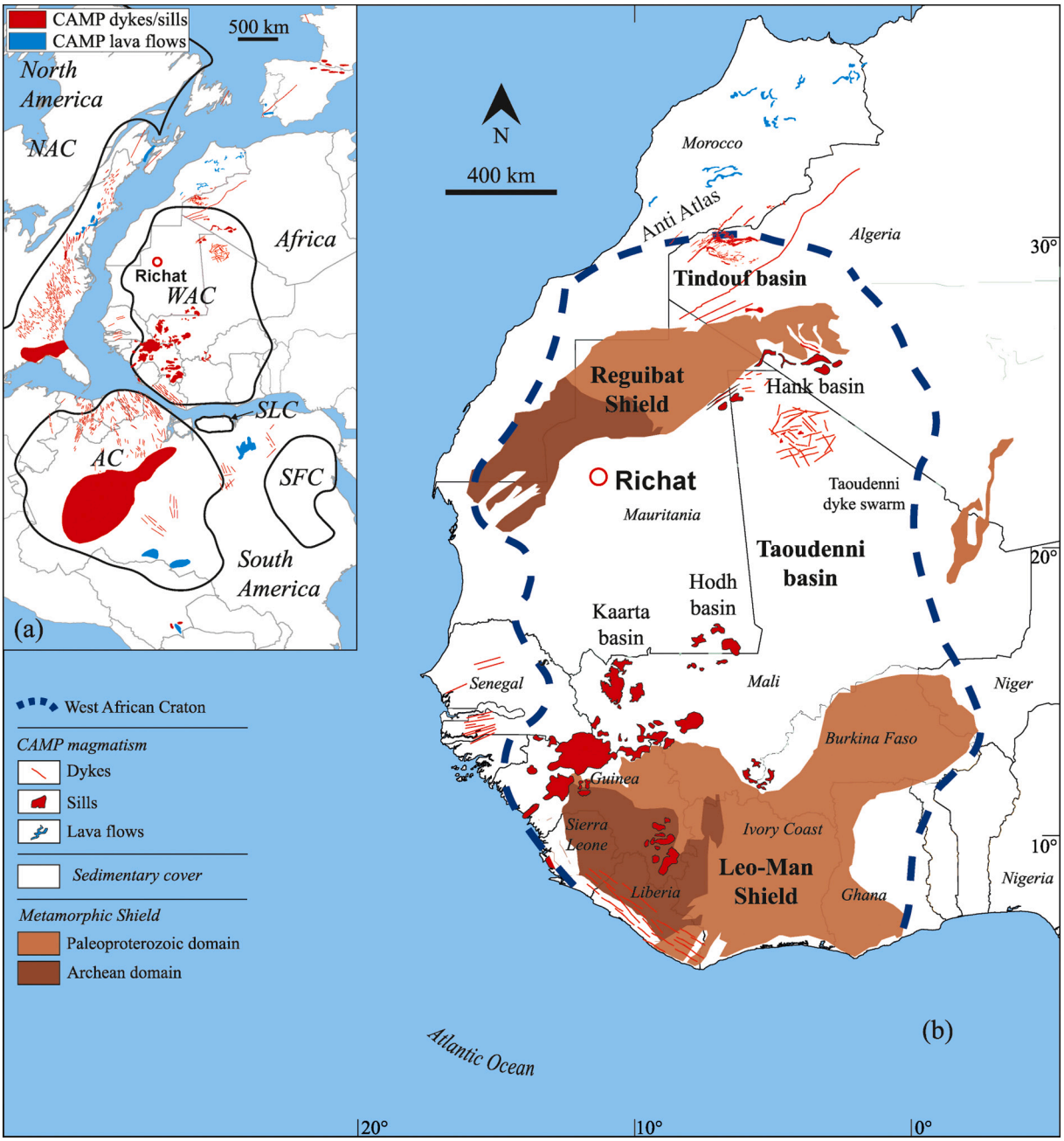


**Fig. 7.** Schematic geological map of NW-Africa with distribution of CAMP remnants after Boscaini et al. (2022) with location of the Richat structure. Insert: sketch map of the CAMP (light grey) in pre-drift position, with location of the Richat structure.

### *7.2. The eye of Africa: an open window on the Central Atlantic Magmatic Province (CAMP)*

Our numerical models suggest a crystallization age between ca. 230 and 201 and warrants further exploration of the possibility that Richat gabbroic rocks are associated with CAMP magmatism whose peak activity is at 201 Ma (Marzoli et al., 2018). Chemical similarities between both events were suggested first by Trompette (1968) who compared the Richat gabbros with dolerites from western Mali (now known as belonging to CAMP, Boscaini et al., 2022). More recently, Matton and Jébrak (2014) mentioned similarities between the Richat gabbros and CAMP tholeiites from Mali and Guinea, but they did not consider that they might be coeval.

To develop this further, we compared the new chemical analyses performed on seven gabbroic samples from the inner and outer rings of the Richat complex (Table 1) with nearby CAMP intrusives (Fig. 7) from Moroccan Anti-Atlas (Marzoli et al., 2019), Kaarta basin in western Mali (Boscaini et al., 2022), and Hank basin in northern Mauritania (Boscaini et al., 2022). As shown in Fig. 3, the Richat gabbroic rocks have major element compositions similar to those of the low-$TiO_2$ group of CAMP intrusives. Trace element compositions are also very similar to those of the CAMP with (i) same rare earth element patterns slightly enriched in LREE (Fig. 4a) and (ii) similar positive Pb anomalies and low concentrations of Nb and Ta for the outer gabbro (Fig. 4b). In detail, the slight difference in LREE enrichment that distinguishes the outer and inner gabbros matches similar differences between two CAMP groups as defined by Marzoli et al. (2018). Specifically, the Richat outer gabbros can be assigned to the Prevalent group of CAMP, as with the dolerites from Hank sills, whereas the inner gabbros are more akin to the Tiourjdal CAMP group, as with the rocks from the Kaarta sill (Fig. 8).

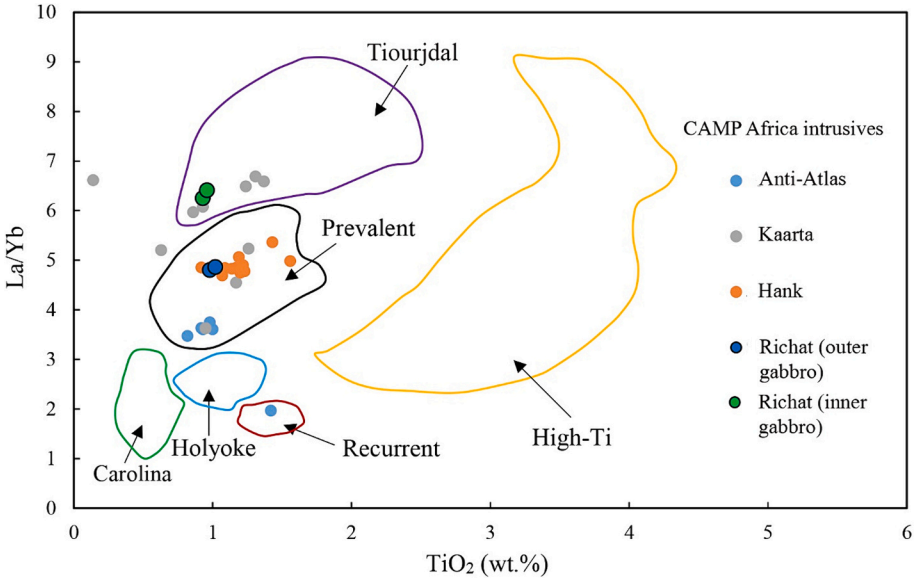


**Fig. 8.** La/Yb versus $TiO_2$ diagram showing the chemical similarity of the outer and inner gabbros from the Richat structure with the two main groups of CAMP magmas in NW-Africa (Prevalent and Tiourjdal groups, respectively). CAMP geochemical groups are from Marzoli et al. (2018).

These chemical similarities, reinforced by the possibility that the gabbroic rocks from the outer ring could be indeed ~201 Ma-old, accordingly with the peak activity of CAMP (Marzoli et al., 2018), raise the intriguing possibility that the earliest Richat magmas were emplaced in the geodynamical context of the Central Atlantic Magmatic Province. In this respect, the localization of the Richat complex is worthy of attention, considering waveform tomography models that image the deep architecture of the lithosphere beneath West Africa (Boscaini et al., 2022; Celli et al., 2020). The Richat gabbros are seen to lie around the edge of the thick lithospheric root of the West African Craton, in accordance with other CAMP outcrops in Taoudenni (Verati et al., 2005), Hodh (Davies et al., 2017) Hank and Kaarta areas (see Fig. 7 of Boscaini et al., 2022). Such boundary zones between a thick cratonic keel and a relatively thinner lithosphere likely favoured preferential asthenospheric mantle upwelling and partial melting generating CAMP magmas. That agrees with other igneous settings, such as the Eastern branch of the East African rift in Northern Tanzania (Koptev et al., 2016; Le Gall et al., 2021). Hence, our $^{40}Ar/^{39}Ar$ and geochemical data, along with our observations on the geodynamic configuration, all together support the idea that the first igneous event preserved in the Richat Structure indeed belongs to the CAMP system.

### *7.3. Implications of two distinct igneous events over 100 My for the Richat history*

Our results resolve one main issue regarding the Richat complex, i.e. coexisting tholeiites and carbonatites which are clearly shown to be of different age and therefore unrelated. This implies a two-stage igneous history, separated by ca. 100 Ma (Fig. 9). However, there are still some issues pending on which the age of the concentric structure (the so-called Eye of Africa) depends: i) were the gabbros emplaced as ring-dykes or sills? ii) when did the doming responsible for the concentric structure occur?

Even if the existence of two ring dykes associated with an underlying central intrusion has been shown recently to be compatible with geophysical modelling (Abdeina et al., 2021), this scenario is contradicted by several lines of evidence. i) Field observations (in spite of poor exposures) point to concordant relationships between the gabbros and the sedimentary country rocks, a feature that would favour the sill hypothesis (O'Connor et al., 2004; Trompette, 1968). ii) Assuming that the gabbros are CAMP-related rocks (see above), it is noteworthy that ring-dyke structures (and associated doming) have never been documented so far in the CAMP system. Instead, CAMP concordant sill intrusions are ubiquitous, as exemplified in the Hank basin (Boscaini et al., 2022), ca. 500 km NE of the Richat area (Fig. 7). Accordingly, the Richat gabbros are here regarded as CAMP-related sills, which intruded into horizontal or gently dipping sedimentary country rocks in late Triassic.

Since sills injection into sediments does not necessarily produce any circular structure, the latter is thus assumed to postdate the end Triassic sill event and to be related to a younger (ca. 100 Ma-old) igneous event, coeval to karst collapse, central breccia and formation of analcimolites. At that time, a central alkaline intrusion was emplaced, possibly related to the Peri-Atlantic Alkaline Pulse event as defined by Matton and Jébrak (2009). It triggered a localized uprise and doming process responsible for the nowadays observed ring-like gabbros and concentric structure of their sedimentary country rocks, due to subsequent erosional effects.

The development of domal structures in sedimentary piles intruded by igneous plug-like bodies has long been documented by numerical modelling (Roman-Berdiel et al., 1995) and natural examples observed in various tectonic settings, such as the CAMP system (Tindouf basin, e.g. Hachemaoui et al., 2022), or the East African rift system in SE Afar (Djibouti, e.g. Le Gall et al., 2010) and in North Kenya, e.g. Le Gall et al., 2005). In the present case, the Richat dome is further dissected by a network of variously oriented faults which post-date the central breccia. This brittle strain is assumed to have accompanied elastic bending of the overburden, in response to the upward driving force of the magma at a late stage of the Cretaceous intrusive event. It is noteworthy that the submeridian fault network nearly parallels the N10–30°E carbonatitic dyke pattern, Cretaceous in age. Assuming the synmagmatic origin of part of the fault network in the Richat area thus suggests that the emplacement of the Cretaceous intrusion occurred at a relatively shallow level, largely above the crustal brittle/ductile transition.

The composition of this still buried intrusion is unknown but its geophysical signature is compatible with a mafic magma (Abdeina et al., 2021). As an alternative to our previous interpretation, it might be unrelated to the gabbros if we consider the latter as CAMP sills. Instead, this Cretaceous intrusion would be connected with both the carbonatitic dyke swarm and the northern kimberlite plug, all dated at around 99 Ma (Fig. 1). Moreover, the subsurface arrival of alkaline magma triggered an intense hydrothermal activity, particularly at the center of the Richat complex (a localized effect that the CAMP tholeiitic magmas were

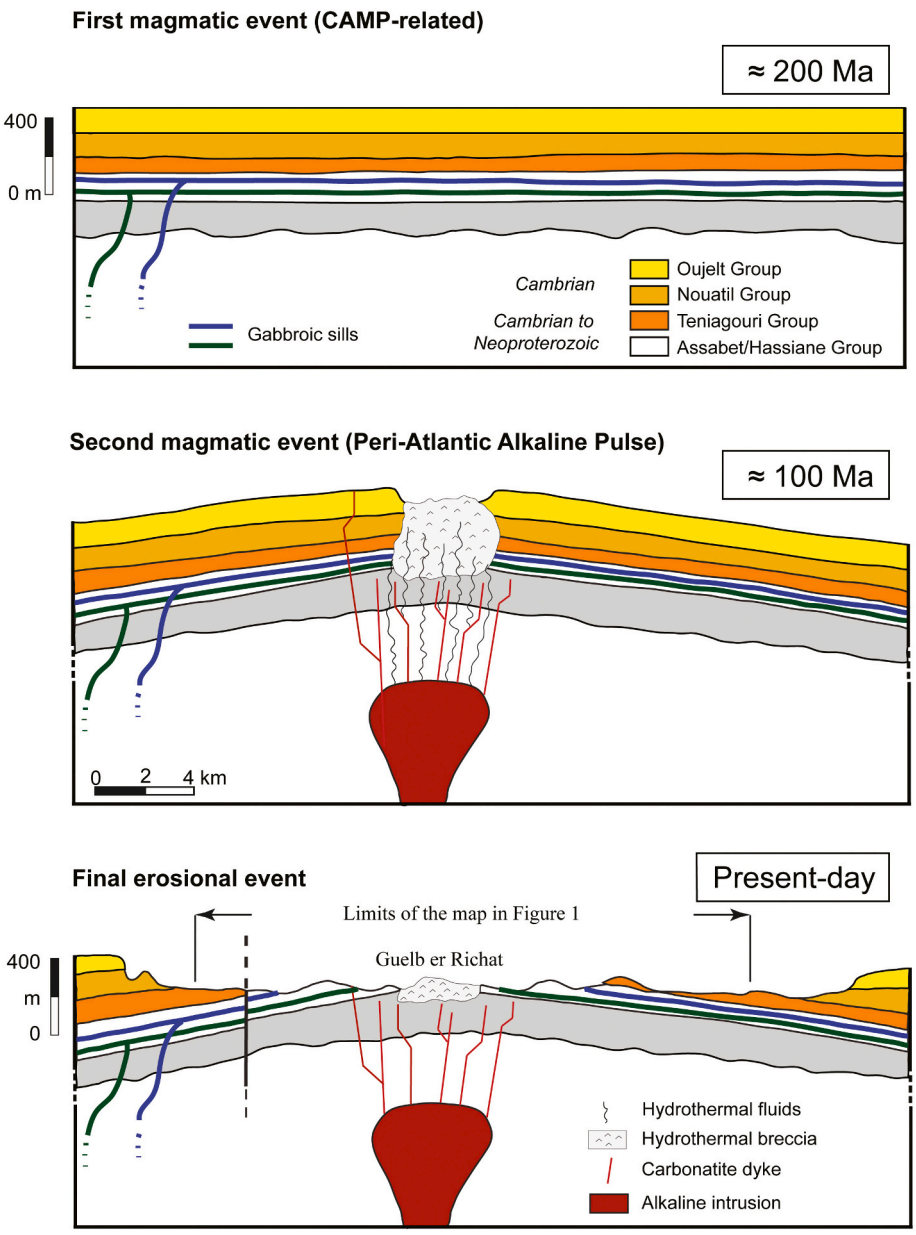


**Fig. 9.** Three-stage tectono-magmatic model of the Richat structure. The stratigraphic and structural data (strata dip) are derived from the geological map of O'Connor et al. (2004). Vertical exaggeration = 10. For easy reading, the lithostratigraphy of the metasedimentary host-rocks has been simplified and the Quaternary deposits are not shown. The vertical dimension of the section is cross-cut in order to show the top of the buried plug-like intrusion (from Abdeina et al., 2021). Sections not oriented.

unable to produce), provoking a karst dissolution and collapse of the overlying carbonate sediments along with the formation of a central breccia in which newly formed K-feldspars were dated at 98.2 ± 2.6 Ma (Matton et al., 2005). These hydrothermal fluids also generated the analcimolites observed NE and SW of the central zone (Fig. 1). Whether these analcimolites derived from sediments (O'Connor et al., 2004; Trompette, 1968) or rhyolites supposed to represent the volcanic expression of the alkaline intrusion (Bardossy et al., 1963; Matton and Jébrak, 2014) is beyond the scope of this paper. The hydrothermal fluids released from the Cretaceous intrusion have also left their imprint on some of the gabbros (in addition to previous CAMP-related alteration), as revealed by the presence of secondary nepheline, analcime and cancrinite (O'Connor et al., 2004; Trompette, 1968), i.e. minerals diagnostic of an alkaline affinity. However, such secondary minerals have not been observed in the gabbros selected for the present study.

## 8. Conclusions

This work presents the first $^{40}Ar/^{39}Ar$ age determination and new geochemical data on the two gabbroic ring-like bodies of the Richat complex, the so-called Eye of Africa. These results shed new light on the remaining outstanding issue of coexisting tholeiitic and carbonatitic (alkaline) magmas and allow to reconsider the geological evolution of the Richat intrusion. Our main conclusions are the following:

- $^{40}Ar/^{39}Ar$ data are compatible with two possible scenarios suggesting approximate formation ages of either ~230 Ma or ~ 200 Ma for the intrusion of the two gabbroic bodies. The second scenario, if correct, is in agreement with the intrusion belonging to the 201 Ma Central Atlantic Magmatic Province (CAMP).

- The two gabbros share similar tholeiitic major and trace element compositions with the two main geochemical groups of CAMP magmas in northwest Africa.
- The gabbros were therefore intruded as CAMP sills concordant with the Late Proterozoic/Lower Paleozoic sedimentary cover of the Taoudenni basin. They lie around the edge of the thick lithospheric root of the West African Craton as other CAMP sills/dykes complexes in Mauritania (Hank and Hodh) and Mali (Taoudenni and Kaarta).
- Ca. 100 My later, the intrusion of a carbonatitic/alkaline magma triggered a doming of the gabbros and their country rocks, followed by a subsequent erosion resulting in the actual annular structure of the Richat complex.
- The Richat Structure is therefore the result of two independent (separated by ca.100 My) tholeiitic and alkaline igneous events (Fig. 9). The former represents the end Triassic CAMP large igneous province, whereas the latter presumably belongs to the Cretaceous Peri-Atlantic Alkaline Pulse (PAAP).

Supplementary data to this article can be found online at https://doi.org/10.1016/j.lithos.2024.107698.

## CRediT authorship contribution statement

**El Houssein Abdeina:** Data curation, Investigation, Visualization, Writing – original draft, Writing – review & editing. **Fred Jourdan:** Data curation, Formal analysis, Methodology, Software, Validation, Writing – original draft, Writing – review & editing. **Gilles Chazot:** Conceptualization, Formal analysis, Investigation, Project administration, Supervision, Validation, Visualization, Writing – original draft, Writing – review & editing. **Hervé Bertrand:** Formal analysis, Investigation, Validation, Writing – original draft, Writing – review & editing. **Bernard Le Gall:** Conceptualization, Formal analysis, Investigation, Writing – original draft, Writing – review & editing.

## Declaration of competing interest

The authors declare that they have no known competing financial interests or personal relationships that could have appeared to influence the work reported in this paper.

## Acknowledgments

The authors are grateful to Greg Shellnutt, Editor-in-Chief of Lithos and to Nick Mortimer and an anonymous reviewer for their interesting and constructive comments. The authors are grateful to the French Embassy, via the SCAC (Service de Coopération et d'Action Culturelle), at Nouakchott for supporting the 4-month mobility of EA in Brest (France).

## References

Abdeina, E.H., Bazin, S., Chazot, G., Bertrand, H., Le Gall, B., Youbi, N., Boumehdi, M.A., 2021. Geophysical modelling of the deep structure of the Richat magmatic intrusion (northern Mauritania): insights into its kinematics of emplacement. Arab. J. Geosc. 14, 1–13.

Albarede, F., 1992. How deep do common basaltic magmas form and differentiate? J. Geophy. Res. Solid Earth 97 (B7), 10997–11009.

Bardossy, G., Monod, T., Pomerol, C., 1963. Decouverte d'analcimolites d'origine endogène dans les Richat (Adrar mauritanien). C. R. Acad. Sci. 256, 3934–3936.

Boscaini, A., Marzoli, A., Bertrand, H., Chiaradia, M., Jourdan, F., Faccenda, M., Durán, L.S., 2022. Cratonic keels controlled the emplacement of the Central Atlantic Magmatic Province (CAMP). Earth Planet. Sci. Lett. 584, 117480.

Boussaroque, J.L., 1975. Étude des analcimolites des Richat (Adrar de Mauritanie) [Ph.D. thesis]. Univ. Paris VI, Paris, p. 105.

Cailleux, A., Guillemaut, A., Pomerol, C., 1964. Présence de coésite, indice de hautes pressions, dans l'accident circulaire des Richat (Adrar mauritanien). C. R. Acad. Sci. 258, 5488–5490.

Celli, N.L., Lebedev, S., Schaeffer, A.J., Ravenna, M., Gaina, C., 2020. The upper mantle beneath the South Atlantic Ocean, South America and Africa from waveform tomography with massive data sets. Geophys. J. Inter. 221, 178–204.

Cotten, J., Le Dez, A., Bau, M., Caroff, M., Maury, R., Dulski, P., Fourcade, S., Bohn, M., Brousse, R., 1995. Origin of anomalous rare-earth element and yttrium enrichments in subaerially exposed basalts: evidence from French Polynesia. Chem. Geol. 119, 115–138.

Davies, J.H., Marzoli, A., Bertrand, H., Youbi, N., Ernesto, M., Schaltegger, U., 2017. End-Triassic mass extinction started by intrusive CAMP activity. Nature Comm. 8 (1), 15596.

Dietz, R.S., Fudali, R., Cassidy, W., 1969. Richat and Semsiyat domes (Mauritania); not astroblemes. Geol. Soc. Am. Bull. 80, 1367–1372.

Bidaut, H., Durandau, A., 1962. Phénomènes volcaniques dans les « Richat » (République Islamique de Mauritanie). C. R. Acad. Sci. 254, 1119–1120.

Fudali, R.F., 1973. Origin of the analcime-bearing rocks of Richat. In: Monod, T., Pomerol, C. (Eds.), Contributions à l'étude de l'accident circulaire des Richat (Adrar de Mauritanie). Sci. Terre Mem. 28, Nancy, pp. 97–105.

Hachemaoui, O., Chabou, M.C., Vertai, C., Bersi, M., 2022. The evolution of the Central Atlantic Magmatic Province (CAMP) plumbing system and its possible environmental effects during the Triassic-Jurassic transition: Insights from doleritic pipes of the Tindouf basin, SW Algeria. Gond. Res. 107, 370–394.

Jiang, Q., Jourdan, F., Olierook, H.K., Merle, R.E., Verati, C., Mayers, C., 2021. $^{40}Ar/^{39}Ar$ dating of basaltic rocks and the pitfalls of plagioclase alteration. Geochim. Cosmochim. Acta 314, 334–357.

Jourdan, F., Eroglu, E., 2017. 40Ar/39Ar and (U-Th)/He model age signatures of elusive Mercurian and Venusian meteorites. Meteor. Planet. Sci. 52 (5), 884–905.

Jourdan, F., Renne, P.R., 2007. Age calibration of the Fish Canyon sanidine 40Ar/39Ar dating standard using primary K–Ar standards. Geochim. Cosmochim. Acta 71 (2), 387–402.

Jourdan, F., Marzoli, A., Bertrand, H., Cirilli, S., Tanner, L.H., Kontak, D.J., Bellieni, G., 2009. 40Ar/39Ar ages of CAMP in North America: Implications for the Triassic–Jurassic boundary and the 40K decay constant bias. Lithos 110 (1–4), 167–180.

Jourdan, F., Timms, N.E., Eroglu, E., Mayers, C., Frew, A., Bland, P.A., Yada, T., 2017. Collisional history of asteroid Itokawa. Geology 45 (9), 819–822.

Koppers, A.A., 2002. ArArCALC-software for $^{40}Ar/^{39}Ar$ age calculations. Comput. Geosci. 28 (5), 605–619.

Koptev, A., Burov, E., Calais, E., Leroy, S., Gerya, T., Guillou-Frottier, L., Cloetingh, S., 2016. Contrasted continental rifting via plume-craton interaction: applications to Central East African Rift. Geosci. Front. 7 (2), 221–236.

Le Gall, B., Vétel, W., Morley, C.K., 2005. Inversion tectonics during continental rifting: the Turkana Cenozoic rifted zone, northern Kenya. Tectonics 24 (2). https://doi.org/10.1029/2004TC001637.

Le Gall, B., Daoud, M.A., Maury, R.C., Rolet, J., Guillou, H., Sue, C., 2010. Magma-driven antiform structures in the Afar rift: the Ali Sabieh range, Djibouti. J. Struct. Geol. 32 (6), 843–854. https://doi.org/10.1016/j.jsg.2010.06.007.

Le Gall, B., Gama, R., Koptev, A., Chazot, G., Boniface, N., Loget, N., Hautot, S., 2021. The anomalously-propagating South Kenya rift in the context of the North Tanzanian Divergence zone, East Africa. Tectonophys 814. https://doi.org/10.1016/j.tecto.2021.228968.

Lee, J.Y., Marti, K., Severinghaus, J.P., Kawamura, K., Yoo, H.S., Lee, J.B., Kim, J.S., 2006. A redetermination of the isotopic abundances of atmospheric Ar. Geochim. Cosmo. Acta 70 (17), 4507–4512.

Leterrier, J., Maury, R., Thonon, P., Girad, D., Marchal, M., 1982. Clinopyroxene composition as a method of identification of the magmatic affinities of paleoseries. Earth Planet. Sci. Lett. 59, 139–154.

Li, Z.-X.A., Lee, C.-T.A., 2006. Geochemical Investigation of Serpentinized Oceanic Lithospheric Mantle in the Feather River Ophiolite, California: Implications for the Recycling Rate of Water by Subduction. Chem. Geol. 235, 161–185. https://doi.org/10.1016/j.chemgeo.2006.06.011.

Marzoli, A., Callegaro, S., Dal Corso, J., Davies, J.H., Chiaradia, M., Youbi, N., Bertrand, H., Reisberg, L., Merle, R., Jourdan, F., 2018. The Central Atlantic magmatic province (CAMP): A review. In: Tanner, L.H. (Ed.), The LateTriassic World. Topics in Geobiology 46. Springer, Heidelberg, pp. 91–125.

Marzoli, A., Bertrand, H., Youbi, N., Callegaro, S., Merle, R., Reisberg, L., Chiaradia, M., Brownlee, S., Jourdan, F., Zanetti, A., Davies, J.H.F.L., Cuppone, T., Mahmoudi, A., Medina, F., Renne, P.R., Bellieni, G., Crivellari, S., El Hachimi, H., Bensalah, M.K., Meyzen, C.M., Tegner, C., 2019. The Central Atlantic Magmatic Province (CAMP) in Morocco. J. Pet. 60 (5), 945–996.

Matton, G., 2008. Le complexe Crétacé du Richat (Mauritanie) : Un processus alcalin péri-Atlantique. Ph.D. Université du Québec à Montréal, p. 173.

Matton, G., Jébrak, M., 2009. The cretaceous Peri-Atlantic Alkaline Pulse (PAAP): deep mantle plume origin or shallow lithospheric breakup? Tectonoph 469, 1–12.

Matton, G., Jébrak, M., 2014. The "eye of Africa" (Richat dome, Mauritania): an isolated cretaceous alkaline–hydrothermal complex. J. Af. Earth Sci. 97, 109–124.

Matton, G., Jébrak, M., Lee, J.K.W., 2005. Resolving the Richat enigma: doming and hydrothermal karstification above an alkaline complex. Geology 33, 665–668.

McDonough, W.F., Sun, S.S., 1995. The composition of the Earth. Chem. Geol. 120, 223–253.

Netto, A.M., Fabre, J., Poupeau, G., Champemmois, M., 1992. Datations par traces de fissions de la structure circulaire des Richats. C. R. Acad. Sci. 314, 1179–1186.

O'Connor, E.A., Pitfield, P.E.J., Schofield, D.I., Coats, S., Waters, C., Powell, J., Ford, J., Clarkel, S., Gillespie, M., 2004. Rapport Administratif des cartes géologiques et gîtologiques à 1/200 000 et 1/500 000 du Nord-Ouest de la Mauritanie. DMG, Ministère des Mines et de l'Industrie, Nouakchott, p. 408.

Poupeau, G., Fabre, J., Labrin, E., Azdimoussa, A., Netto, A.M., Monod, T., 1996. Nouvelles datations par traces de fission de la structure circulaire des Richat (Mauritanie). Mém. Serv. Géol. Alg. 8, 231–236.

Renne, P.R., Balco, G., Ludwig, K.R., Mundil, R., Min, K., 2011. Response to the comment by WH Schwarz et al. on "Joint determination of 40K decay constants and 40Ar*/40K for the Fish Canyon sanidine standard, and improved accuracy for 40Ar/39Ar geochronology" by P.R. Renne et al. (2010). Geochim. Cosmochim. Acta 75 (17), 5097–5100.

Renne, P.R., Deino, A.L., Hilgen, F.J., Kuiper, K.F., Mark, D.F., Mitchell, W.S., Morgan, L. E., Mundil, R., Smit, J., 2013. Time scales of critical events around the Cretaceous-Paleogene boundary. Science 339, 684–687.

Roman-Berdiel, T., Gapais, D., Brun, J.P., 1995. Analigue models of laccolith formation. J. Struct. Geol. 9, 1337–1346.

Scibiorski, E., Jourdan, F., Mezger, K., Tohver, E., Vollstaedt, H., 2021. Cryptic excess argon in metamorphic biotite: Anomalously old 40Ar/39Ar plateau dates tested with Rb/Sr thermochronology and Ar diffusion modelling. Geochim. Cosmo. Acta 315, 1–23.

Sedigh, M.E., Ouali, H., Jébrak, M., Mokhtari, A., 2024. Bulk composition and O–C isotope constraints on the petrogenesis of Richat carbonatites (Mauritania). J. Afr. Earth Sci. 209, 105126 https://doi.org/10.1016/j.jafrearsci.2023.105126.

Trompette, R., 1968. Les dolérites de l'Adrar de Mauritanie et le problème des analcimolites des Richat (Sahara occidental). Ann. Fac. Sv. Dakar 115–132.

Verati, C., Jourdan, F., 2014. Modelling effect of sericitization of plagioclase on the $^{40}K/^{40}Ar$ and 40Ar/39Ar chronometers: implication for dating basaltic rocks and mineral deposits. Geol. Soc., London, Sp. Pub. 378 (1), 155–174.

Verati, C., Bertrand, H., Féraud, G., 2005. The farthest record of the Central Atlantic Magmatic Province into West Africa craton: Precise 40Ar/39Ar dating and geochemistry of Taoudenni basin intrusives (northern Mali). Earth Planet. Sci. Lett. 235 (1–2), 391–407.

Woolley, A.R., Rankin, A.H., Elliott, C.J., Bishot, A.C., Niblett, D., 1984. Carbonatite dykes from the Richat dome, Mauritania, and the genesis of the dome. Indian Min. 189–207.